ELSEVIER

Chemical Geology 177 (2001) 43–66

CHEMICAL GEOLOGY
INCLUDING
ISOTOPE GEOSCIENCE

www.elsevier.com/locate/chemgeo

Elevated carbon dioxide flux at the Dixie Valley geothermal field, Nevada; relations between surface phenomena and the geothermal reservoir

Deborah Bergfeld [a,*], Fraser Goff [a], Cathy J. Janik [b]

[a] *Los Alamos National Laboratory EES-1, MS D462, Los Alamos, NM 87545, USA*
[b] *U.S. Geological Survey, MS 910, 345 Middlefield Road, Menlo Park, CA 94025, USA*

Received 10 May 2000; accepted 20 June 2000

Abstract

In the later part of the 1990s, a large die-off of desert shrubs occurred over an approximately 1 km^2 area in the northwestern section of the Dixie Valley (DV) geothermal field. This paper reports results from accumulation-chamber measurements of soil CO_2 flux from locations in the dead zone and stable isotope and chemical data on fluids from fumaroles, shallow wells, and geothermal production wells within and adjacent to the dead zone. A cumulative probability plot shows three types of flux sites within the dead zone: locations with a normal background CO_2 flux (7 g m^{-2} day^{-1}); moderate flux sites displaying "excess" geothermal flux; and high flux sites near young vents and fumaroles. A maximum CO_2 flux of 570 g m^{-2} day^{-1} was measured at a location adjacent to a fumarole. Using statistical methods appropriate for lognormally distributed populations of data, estimates of the geothermal flux range from 7.5 t day^{-1} from a 0.14-km^2 site near the Stillwater Fault to 0.1 t day^{-1} from a 0.01-km^2 location of steaming ground on the valley floor. Anomalous CO_2 flux is positively correlated with shallow temperature anomalies. The anomalous flux associated with the entire dead zone area declined about 35% over a 6-month period. The decline was most notable at a hot zone located on an alluvial fan and in the SG located on the valley floor.

Gas geochemistry indicates that older established fumaroles along the Stillwater Fault and a 2-year-old vent in the lower section of the dead zone discharge a mixture of geothermal gases and air or gases from air-saturated meteoric water (ASMW). Stable isotope data indicate that steam from the smaller fumaroles is produced by $\approx$100°C boiling of these mixed fluids and reservoir fluid. Steam from the Senator fumarole (SF) and from shallow wells penetrating the dead zone are probably derived by 140°C to 160°C boiling of reservoir fluid. Carbon-13 isotope data suggest that the reservoir CO_2 is produced mainly by thermal decarbonation of hydrothermal calcite in veins that cut reservoir rocks.

Formation of the dead zone is linked to the reservoir pressure decline caused by continuous reservoir drawdown from 1986 to present. These reservoir changes have restricted flow and induced boiling in a subsurface hydrothermal outflow plume extending from the Stillwater Fault southeast toward the DV floor. We estimate that maximum CO_2 flux in the

* Corresponding author. Tel.: +1-505-667-1812; fax: +1-505-665-3285.
E-mail address: debberg@cybermesa.com (D. Bergfeld).

0009-2541/01/$ - see front matter. Published by Elsevier Science B.V.
PII: S0009-2541(00)00381-8

upflow zone along the Stillwater Fault in 1998 was roughly seven to eight times greater than the pre-production flux in 1986. The eventual decline in CO_2 flux reflects the drying out of the outflow plume. Published by Elsevier Science B.V.

Keywords: Carbon dioxide; Flux; Soil gas; Gas geochemistry; Stable isotopes; Geothermal system; Dixie Valley, NV

1. Introduction

The Dixie Valley (DV) geothermal field in west-central Nevada feeds a double-flash power plant that produces 62 MW of electric power. Over the past 10 years, fluid levels and pressures in the reservoir have decreased in spite of reinjection of spent brine at locations along the margin of the production zone. In August 1996, a set of new ground fractures was identified at a location on the valley floor about 1.5 km northwest of the geothermal field (S. Johnson, 2000, personal communication). Several weeks later, it was noted that vegetation appeared distressed in an area south of these cracks and on lower sections of nearby alluvial fans. In October, when the ambient air temperature decreased, a second set of ground cracks near the dying plants was observed to be producing steam. During the spring of 1997, plants around the steaming ground area did not leaf out and were determined to be dead.

In the past decade, CO_2 soil–gas investigations resembling the type described herein have been conducted in volcanic areas to estimate total CO_2 flux from vents and diffuse flank emissions (Allard et al., 1991; Chiodini et al., 1996), and to identify tectonic structures associated with volcanic degassing (Barberi and Carapezza, 1994; Giammanco et al., 1997). In the U.S., anomalously high CO_2 flux has been associated with areas of tree-kill at Mammoth Mountain, CA (Farrar et al., 1995, 1999; Gerlach et al., 1998; McGee and Gerlach, 1998). The formation of a dead zone at DV caused concern that large changes were occurring in the top of the geothermal reservoir. The CO_2 flux study was initiated to provide supportive data to an ongoing geochemical investigation of reservoir conditions and to see if a thorough examination of the surface phenomena could provide information about the processes occurring at depth.

This paper presents CO_2 flux and soil temperature data from parts of the dead zone in the northern portion of the geothermal field, and presents supporting gas and stable isotope analyses of geothermal and associated fluids from DV. These data are used to determine the source of dead zone steam and carbon dioxide, to quantify the amount of geothermal CO_2 that was being emitted, and to estimate the volume of boiling geothermal fluids necessary to produce the CO_2 in the dead zone.

2. Geologic setting

2.1. DV geothermal field

DV, located in west-central Nevada (Fig. 1), is the southernmost geothermal system in a region of elevated heat flow known as the Battle Mountain High. The valley is an asymmetric, northeast trending graben bounded by the Stillwater range on the west and the Clan Alpine range on the east (Anderson et al., 1983; Waibel, 1987). The geothermal field is located along the western, deeper margin of DV

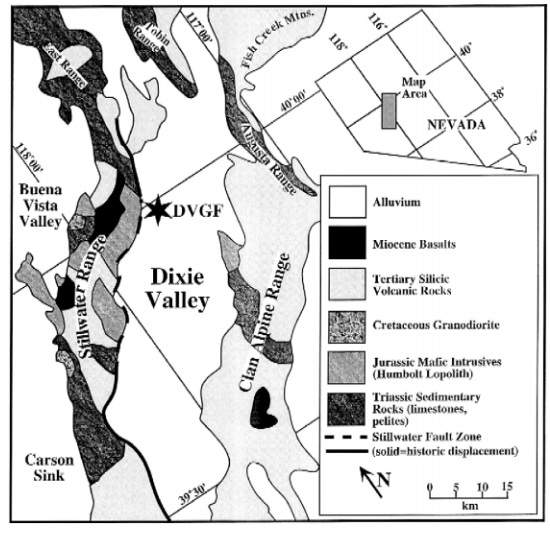

Fig. 1. Generalized geologic map of the region around DV, after Nimz et al. (1999). DVGF = Dixie Valley geothermal field.

near the Stillwater Fault. In some geothermal wells Tertiary basin-fill sediments are up to 2000 m thick (Forster et al., 1997). Movement along the presently active Stillwater Fault has produced roughly 2.9 km of vertical offset between the Stillwater range and the floor of DV over the past 10 Ma (Okaya and Thompson, 1985). As such, the rock units exposed in the Stillwater range are mostly the same as those penetrated by geothermal wells in the basin. The rock units consist of repeated, thrusted sequences of Triassic and Jurassic marine metasedimentary rocks and a Jurassic gabbroic complex (Humbolt Lopolith) that were later intruded by a Cretaceous granodiorite (Speed, 1976). The Mesozoic rocks are unconformably overlain and intruded by the Miocene Table Mountain Basalt. In the basin, this basalt hosts the upper geothermal reservoir at depths between 2300 and 2700 m (Lutz et al., 1997). The main geothermal reservoir between 2830 and 3330 m depth is hosted in fractured Jurassic rocks within the hanging wall of the Stillwater Fault (Lutz et al., 1997). The average temperature of reservoir fluids is presently about 245°C.

2.2. Surface features and dead zone development

The recently identified dead zone is an area with anomalous plant mortality located in the northwestern part of the geothermal field extending southeast from an area of persistent fumarolic activity along the Stillwater Fault to the valley floor (Fig. 2). The zone encompasses a nearly 1 km^2 area that is comprised of alluvial fan and basin sediments. Plants that grow in the area consist of low-lying woody shrubs (primarily greasewood and shadscale) with interspersed grasses. Fumarolic areas are devoid of woody shrubs; the soil is typically moist and usually displays elevated temperatures ranging up to 97°C. Two

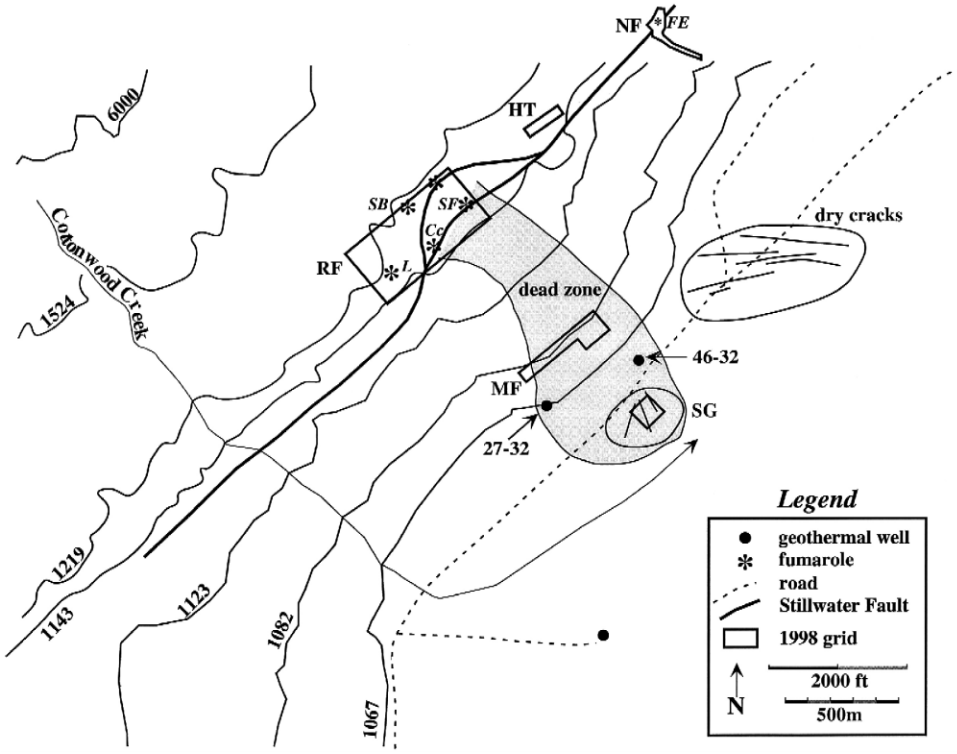

Fig. 2. Map of the northern portion of the DV geothermal field. The dead zone region is highlighted in gray. The topographic contours are in meters. Cc = Calcite fumarole, SF = Senator fumarole, SB = South Bench fumarole, L = Lonely fumarole, FE = Figure Eight fumarole, RF = range front grid, MF = mid-fan grid, SG = steaming ground grid, HT = High Traverse sites and NF = North Fumarole sites. The latter two sites consist of irregularly spaced plots added late in the study.

large fumaroles, Senator fumarole (SF) and Calcite fumarole, as well as a few small fumaroles, appear to predate development of the geothermal field.

Plant mortality in non-fumarolic areas across the upper part of the fan is patchy with increasing die-off at locations near the access road at the fan terminus (Fig. 2). The southernmost set of new ground fractures is located near the fan-valley margin. These cracks are generally positioned in a north–south orientation and the crack depths vary from centimeters to around 0.5 m. During the early stages of our investigation, soil in the cracks was moist and soil temperatures were around 96°C at the bottom of the cracks. During the cool periods of the day, water vapor could be seen rising from the cracks. At the ground surface above and adjacent to the cracks, a thin crust of unidentified brown to white precipitates and/or sublimates was common. Plant mortality in the steaming ground region was almost 100%. During the latter stages of the investigation, the maximum soil temperature recorded at the base of the ground cracks was 80°C and the soil was generally dry. In March 1999, there was no visible steaming ground, and recent observations since that time indicate that there is some new plant growth in the area (S. Johnson, 2000, personal communication).

A second set of ground cracks is located in basin-fill sediments northeast of the steaming ground area (Fig. 2). These cracks are generally oriented in an east–west direction. Except when wetted by precipitation, the soil within the cracks was dry. Maximum depth of these cracks was $\sim$1 m. During the early part of the investigation, these cracks had sharp edges and steep-sided walls and appeared to be very young. As the study progressed, there was some infilling of the cracks due to crumbling of the walls, but large cracks that crossed local roads continued to form throughout the duration of the investigation (D. Benoit, 1999, personal communication). Average soil temperatures at the base of the cracks in the fall of 1997 were about 17°C, similar to temperatures in the surrounding sediments. Compared with the cracks in the steaming ground area, the dry cracks are deeper and more laterally extensive. The plants around the dry cracks are healthy.

3. Methods

3.1. CO_2 flux measurements

Soil CO_2 fluxes were measured using a portable LI-COR brand 6200 infrared gas analyzer (IRGA) linked via a closed loop with a 1 liter accumulation chamber (Fig. 3). The manufacturer reports the analyzer accuracy as $\pm$2 ppm at 1000 ppm CO_2. At elevations of 4000 ft ($\approx$1200 m, the upper elevation

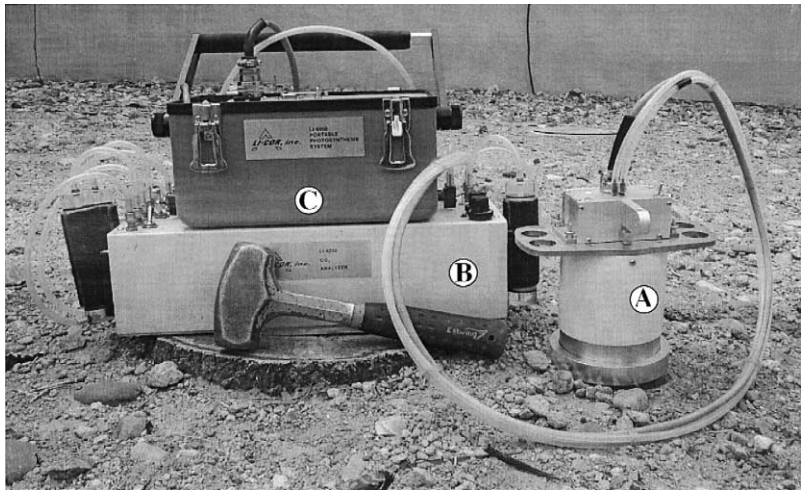

Fig. 3. Photo of the CO_2 flux measurement system. A = Accumulation chamber, B = infrared gas analyzer, C = computer. Hammer is for scale.

of the study area), the upper limit of the analyzer is around 3000 ppm (Demetriades-Shah, 2000, personal communication). Soil gases are pumped from the accumulation chamber to the IRGA for analysis and subsequently returned to the chamber. The IRGA is connected to a computer that records the data at a rate of one sample per second and calculates the flux using,

$$\text{Flux} \approx \left(\frac{\rho V}{A}\right)\left(\frac{\mathrm{d}c}{\mathrm{d}t}\right), \quad (1)$$

where ρ is molar density of air, V is the total volume of the system, $\mathrm{d}c/\mathrm{d}t$ is the rate of change of CO_2 in the chamber, and A is the soil area under the chamber. We report the CO_2 flux as grams of CO_2 per square-meter per day (g m^{-2} day^{-1}).

The CO_2 analyzer was calibrated at the start of each day using a CO_2-free gas and a reference gas containing 1200 ppm CO_2 in air. During this procedure, only small adjustments (0 to 2 ppm) of the calibration were necessary. Throughout the day, the zero measurement was checked, and if necessary, adjusted. Because variations in atmospheric pressure affect the response of the analyzer, a digital barometer was used to monitor pressure throughout the day. Changes in atmospheric pressure do not require recalibration of the instrument and are compensated by entering the new pressure value into the software files.

For most sites, the LI-COR measurement protocol was followed when making flux measurements. The method is designed to most closely replicate natural conditions by reducing the effects of the accumulation chamber on the natural gas diffusion rate. The protocol begins with measurement of the ambient air CO_2 concentration at the soil surface. The accumulation chamber is then placed over the sample location and the sharpened base of the chamber is gently pressed into the ground. We allowed a rest period of approximately 1 min before initiating sample measurement. The chamber gases are then pumped into the analyzer through in-line magnesium perchlorate and soda–lime canisters, which remove water vapor and CO_2, respectively. During this procedure, the decline in the CO_2 concentration is monitored on a digital readout on the computer. After the CO_2 concentration in the chamber falls to near zero, the soda–lime scrub is bypassed and the CO_2 concentration in the chamber increases. As the CO_2 concentration approaches the ambient value, the operator begins to record the data. The data are logged between CO_2 concentrations below, to just above, ambient conditions.

We altered our sampling methods in areas that had very large CO_2 fluxes because it was impossible to reduce the chamber gases below ambient concentrations. In these instances, the flux measurements were initiated immediately upon placing the chamber onto the soil. Flux measurements directly over fumaroles were usually not possible as rapid buildup of CO_2 concentrations in the accumulation chamber immediately overwhelmed the saturation limits of the analyzer.

Replicate flux measurements were taken at approximately one-third of the sample locations. Samples were repeated within a time span of 10 to 15 min. At high flux localities, it was necessary to remove the accumulation chamber from the soil between repetitions. At low and moderate flux locations, the accumulation chamber was not removed from the soil when multiple measurements were performed.

3.2. Site selection

The DV CO_2 study included three field campaigns in October 1997, April 1998, and October 1998. Flux measurements in the first survey were performed to identify areas displaying anomalously high CO_2 emissions. During this survey, a total of 168 individual sites were measured for CO_2 flux over a period of 9 days. Most sites were located along regularly spaced, linear traverses that enclosed or crossed the dead zone. Additional traverses were located along and across splays in the Stillwater Fault and around the dry cracks area. Several short traverses were performed in areas over a kilometer away from the dead zone to obtain the natural background CO_2 flux. All sample locations were flagged for ease in relocation during subsequent field campaigns. Results from this study identified three areas, denoted as the range front (RF), mid-fan (MF) and steaming ground (SG), as locations displaying elevated CO_2 flux (Fig. 2). During the second (8 days) and third (11 days) field campaigns, sample sites

were concentrated in these three areas. When possible, these sites were arranged along regularly spaced grids. As a result of natural obstructions in the terrain (deep ravines and occasional huge boulders), minor irregular spacing occurs in each grid (± 1.5 m), and all grids contained some irregularly spaced sites that were retained from the 1997 investigation.

The RF locality contains the largest grid encompassing roughly 137,500 m^2. The grid is characterized by a total of 82 sample sites using a 50-m spacing interval. One edge of the RF grid is located along a bench on the Stillwater fault zone. The grid extends to the southeast onto upper portions of an alluvial fan. The grid includes a fumarole-rich area that is contiguous with the fault zone. The MF and SG grids have a 25-m spacing interval and include 66 and 25 sample sites covering 26,250 and 10,000 m^2, respectively. The eastern section of the MF grid includes a localized area that is characterized by high soil temperatures. The SG grid is located on the valley floor, contains the new steaming cracks, and has many sites with high soil temperatures.

Two small, irregularly spaced plots, High Traverse (HT, 8 sites) and North Fumarole (NF, 16 sites), were added to the study in the fall 1998 field campaign (Fig. 2). These new areas were identified as having hot ground by an aerial temperature survey (S. Johnson, 1999, personal communication). The locations of the HT and NF sites were along steep portions of the Stillwater range, north of any previously surveyed flux localities. In the 1998 spring and fall field campaigns, the total number of sample sites was 174 and 218, respectively. In this paper, data from all three field campaigns are reported; however, comparisons of flux data from different field campaigns are restricted to samples from the SG, MF, and RF grids during the 1998 field campaigns. The results of the flux measurements are summarized in Figs. 4 and 5 and in Table 1. A table of the individual flux values is available upon request from the first author.

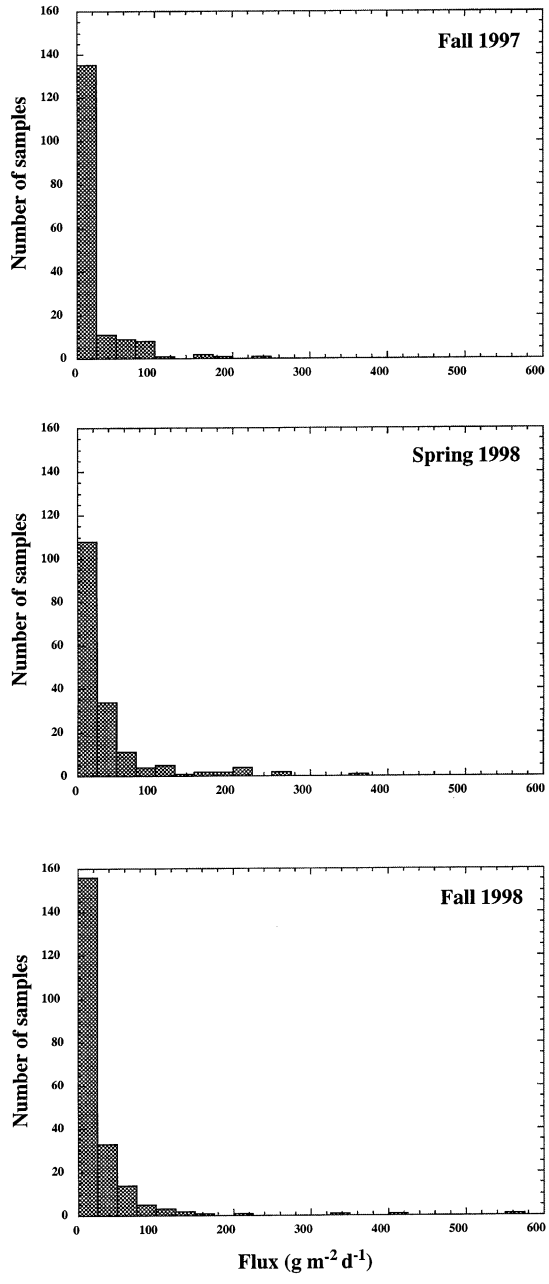

Fig. 4. Histograms of the CO_2 flux data from the three field campaigns.

3.3. Fluid sampling

For gas sampling, doubleport gas collection bottles were prepared in the laboratory using methods described by Fahlquist and Janik (1992). The bottles are partially filled with 4 N NaOH and all head space gases are evacuated. During gas sampling, H_2O, CO_2, H_2S, and NH_3 are absorbed in the caustic solution, while non-absorbable gases (H_2,

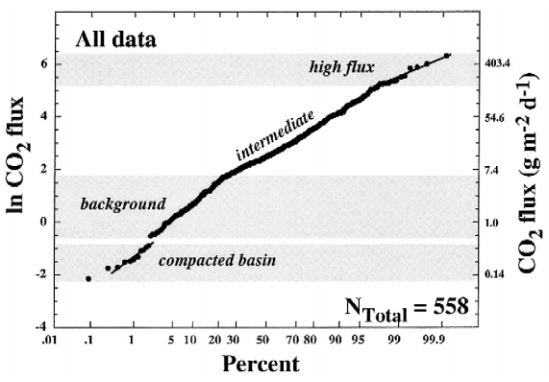

Fig. 5. Cumulative probability plot of the ln CO_2 flux values for all field campaigns. Changes in slope indicate four flux populations.

He, Ar, O_2, N_2 and hydrocarbons) concentrate in the head space of the evacuated bottle.

Gas and steam-condensate samples at fumaroles were collected using an inverted funnel that was placed directly over the vent (Fahlquist and Janik, 1992). Moist soil was mounded around the base of the funnel to prevent atmospheric gases from mixing with the fumarole gases. One end of a piece of vacuum tubing was attached to the funnel and the other end to the gas collection bottle. A hand pump was used to purge air from the funnel and tubing. The fumarole gases (including water vapor) were then collected in the gas bottle. Additional samples of steam were collected by condensing steam to water in 30-ml glass vials for stable isotope analyses.

Fluids from deep geothermal wells were collected at dedicated sampling ports located near the wellheads on horizontal sections of the insulated flow lines. The sampling ports are positioned along upper and lower sections of the flow line for collection of vapor (gas + steam) and brine, respectively. These ports are also the locations where the fluid pressure is measured. To obtain a representative vapor sample, a traversing rod is inserted through the outer wall of the flow line into the vapor stream. Since the fluids are at temperatures well above 100°C the sampling system includes condensing coils (1/4 in. stainless steel tubing) that are placed in water to cool the fluid as it travels from the flow line to the collection bottle. Methods and apparatus to sample fluids from geothermal wells are described by Giggenbach and Goguel (1989) and by Fahlquist and Janik (1992).

4. Results

4.1. CO_2 flux

Measurements of background CO_2 flux at DV were completed during the fall 1997 field campaign, and gave average values of 2 and 7 g m^{-2} day^{-1} for basin and fan areas, respectively. These values are somewhat lower than those typically reported for prairie soils (about 8–11 g m^{-2} day^{-1}; Norman et al., 1992), demonstrating a difference between desert

Table 1
Summary statistics for the SG, MF and RF grids for the two 1998 field campaigns

	Steaming ground		Mid-fan		Range front	
	April	October	April	October	April	October
Number of samples	26	26	63	63	77	77
Flux sum (g m^{-2} day^{-1})	601	331	1284	711	4627	3251
Mean flux (g m^{-2} day^{-1}), μ_{grid}	25.7	14.9	18.8	10.9	61.6	43.5
Variance flux population, s^2_{grid}	2565	1255	150	41	8341	7250
Standard deviation flux population	50.6	35.4	12.2	6.4	91.3	85.1
Standard deviation population mean	9.1	6.2	1.5	0.8	9.6	8.5
Grid flux (kg/day)	257	149	494	287	8464	5975
Background flux (kg/day)	70	70	184	184	963	963
Geothermal flux (kg/day)	187	79	310	103	7501	5013
Percent geothermal flux	72.8%	53.1%	62.8%	36.0%	88.6%	83.9%

SG, MF, and RF grids include 10,000; 26,500; and 137,500 m^2, respectively.
Background flux assumes an average flux at all grids equal to 7 g m^{-2} day^{-1}.

and grassland conditions. All CO_2 flux values around the dry cracks were < 6 g m^{-2} day^{-1}, within the range of the background samples.

The reproducibility of repeated measurements was assessed using the coefficient of variation (CV), which is the standard deviation for the repeated measurements divided by their average value, here expressed as a percent. In the calculations and figures presented in this work, the average flux was used when replicate measurements yielded a CV of less than 20%. The data that generate the higher CVs ($< 7\%$ of all repeated sites) were examined for consistency and checked against field notes. If there were more than two measurements at these sites, the average of the most consistent data was reported. If there were only two measurements, the second flux value was retained. A subset of replicate measurements (RM2 data set, 69 samples out of 213 total), taken from the three grids during the two 1998 field campaigns have a minimum of three flux measurements taken in succession. These data are used in a repeated-measures model below to quantify the variability inherent in the flux measurements (Christensen, 1991).

Histograms of all of the flux data for each field campaign show that most sites exhibit low and moderate fluxes and only a few sites show a very large CO_2 flux (Fig. 4). This type of distribution is common in other types of geochemical studies (Gilbert, 1987) and has been observed in soil CO_2 flux studies at Yellowstone National Park, WY, at Mammoth Mountain, CA, and in portions of Greece and southern Italy where there is an anomalous source of CO_2 at depth (Chiodini et al., 1998; Werner et al., 2000; Gerlach et al., 2001). The largest fluxes measured at DV were from sites near fumaroles and ranged between 360 and 570 g m^{-2} day^{-1}, less than the maximum fluxes reported at the aforementioned areas.

The linear nature of the cumulative probability plot of the natural log (ln) of the CO_2 flux (Fig. 5) suggests that the flux data can be modeled as a lognormal distribution. Sinclair (1974) discussed that in such plots, changes in slope are indicative of separate populations of data. The flux data from DV can be partitioned into four populations. The population of extremely low flux data consists of values from a few sites in compacted basin sediments. The remaining data can be partitioned into background (0.5 to 7 g m^{-2} day^{-1}) and high flux (> 150 g m^{-2} day^{-1}) end members, with an intermediate flux population that overlaps the two end members. The high flux population (except one sample) consists entirely of values measured from sites along traces of the Stillwater fault zone.

In order to estimate the total CO_2 flux for the three gridded areas, it is important to understand the nature of the data distribution. Assumptions of a normal population and calculation of arithmetic averages for the data can lead to overestimation of the total flux (Gilbert, 1987). We tested the hypothesis of a lognormal distribution for the flux data from the 1998 grids following the methods outlined in Gilbert (1987). We used the D'Agostino (1971) test for the grids with > 50 sites and the W test of Shapiro and Wilk (1965) for the SG grid. For all of the grids the hypothesis that the data have a lognormal distribution was found to be acceptable for a 95% confidence interval.

To compare the data from the spring and fall 1998 field campaigns, we calculated the grid means (μ_{grid}) and variances (s^2_{grid}) using only the data from sites that were sampled both times. For each survey, the estimations of μ_{grid} and s^2_{grid} were made assuming a lognormal distribution, using the minimum variance estimators:

$$\mu_{\text{grid}} = \exp\left(\bar{y} + \frac{s_y^2}{2}\right) \tag{2}$$

and

$$s^2_{\text{grid}} = \mu^2_{\text{grid}}\left[\exp\left(s_y^2\right) - 1\right], \tag{3}$$

(Gilbert, 1987) where $\bar{y}$ is the arithmetic mean of ln flux for the population of individual values measured within the grid. We used the repeated-measures model of Christensen (1991) to calculate the flux population variance (s_y^2) in order to include multiple flux values from the RM2 data set with data from sites having only one measurement. Because the model requires a normal distribution for the data, we used the natural log of the flux values for the calculations. The model also assumes that the repeated measurements are equally correlated, which is applicable since our repeated flux data do not show any strong trends with respect to time. The repeated

measures model returns two values for the variance. One value represents the variance for the population of grid data and the second value represents the variance for the repeated measurements. These values were summed to obtain s_y^2 for Eqs. (2) and (3) above, and Eq. (4) below. The results of the statistical calculations are presented in Table 1.

The estimates of the total flux for each grid were calculated by multiplying μ_{grid} by the grid area (Table 1). The background flux component of the total flux was calculated in a similar fashion by assuming $\mu_{\text{background}}$ equals 7 g m^{-2} day^{-1}. The anomalous excess or "geothermal" flux is the difference between the total and background flux values (Table 1). It is arguable that because most of the vegetation in the SG grid is dead, there is no root respiration and therefore a background flux component should not be subtracted from the total flux. To be conservative, we chose to treat the SG data in the same fashion as the MF and RF grids. If there is no natural background CO_2 flux in the SG area, then the geothermal flux we calculated for the grid is a minimum value.

Comparison of the grid data shows mean CO_2 flux values were highest in the RF grid followed by the SG and MF grids. For all grids, the estimated mean flux values were largest in the spring of 1998. To test if the true grid means had declined from spring to fall, we performed a two-sample Student's *t*-test to compare the estimated means for each grid for the two periods. For this comparison, we calculated the standard deviation of the population means $s(\mu_{\text{grid}})$ as:

$$s(\mu_{\text{grid}}) \cong \left[\exp\left(2\bar{y} + \frac{s_y^2}{n}\right)\left[\left(1 - \frac{2s_y^2}{n}\right)^{-(n-1)/2} \times \exp\left(\frac{s_y^2}{n}\right) - \left(1 - \frac{s_y^2}{n}\right)^{-(n-1)}\right]\right]^{0.5}, \quad (4)$$

which is a measure of the uncertainty of the estimated mean (Gilbert, 2000, personal communication). The variables are the same as discussed previously and n is the number of samples. The results of the *t*-test suggest that the means are significantly different (within a 95% confidence interval) and that the CO_2 flux declined between April and October 1998.

To more easily visualize temporal changes in the CO_2 flux, contour plots were made using a computer plotting program (Fig. 6). The contours were generated from the same data sets as discussed above, choosing the default kriging algorithm (with a linear variogram) to produce an evenly spaced grid of flux values from which the contours are drawn. After the grids were constructed, the October grid was subtracted from the April grid to produce a set of grid values that represent changes in the flux between the two periods. Negative contours in Fig. 6 represent areas where the flux was higher in the fall and positive contours represent areas where the flux declined. Parts of the SG and MF grids show essentially no change, but there are declines in the flux that are localized around the steaming cracks and the MF hot zone. The RF grid is more variable with large positive and negative shifts occurring in areas concentrated along the Stillwater fault zone.

Several recent studies have used continuous monitoring devices to examine temporal changes in flux at a single location. These studies have found that short-term temporal variations in flux may be large (Rogie et al., 1998) and that flux at some locations is influenced by changes in barometric pressure (Chiodini et al., 1998). We performed a limited investigation of short-term temporal variations in flux by revisiting five sites on different days during the course of a field campaign. Two background flux sites were located along the perimeter of the SG area. Moderate flux sites were located in the SG and RF grids and one high flux site was located near a crack in the SG grid. The sites were sampled between three and five times each and produced no obvious trends with respect to time. CVs for the short-term temporal measurements were between 21% and 37% with the high flux site showing the greatest variability (Fig. 7). Of the five sites, only the high flux locality showed a possible relation between the flux and atmospheric pressure.

Since the mean flux calculations reported in Table 1 do not include any estimates of short-term variability, we must consider the grid means and the total grid fluxes as estimates of an instantaneous flux. If the two instantaneous total fluxes measured in 1998

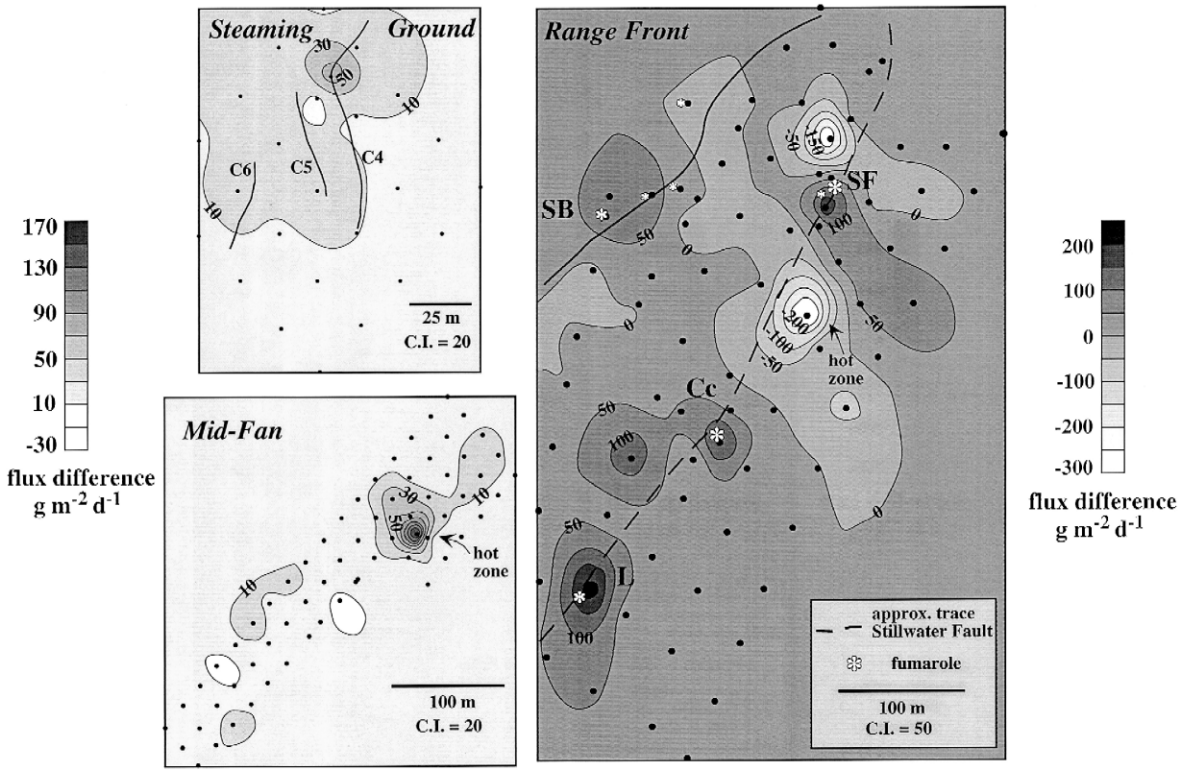

Fig. 6. Differential contour plots of the CO_2 flux for the three grid areas. Flux values from fall 1998 are subtracted from values in spring 1998 to highlight the difference over the two field campaigns. Positive contours delineate areas where the flux declined. Contour interval (in g m^{-2} day^{-1}) is 20 for SG and MF and is 50 for RF. The gray scale for the RF grid differs from the other grids. Steaming ground cracks are numbered C4, C5 and C6. Fumarole abbreviations are as in Fig. 2.

are representative estimates of the long-term trend, then the production of anomalous CO_2 in the SG and MF areas was undergoing a large decline, whereas a smaller decline was occurring in the RF area.

4.2. Soil temperatures

Soil temperature data were taken at each site using a digital thermometer by inserting a temperature probe to a depth of around 15 cm. Soil temperatures at sites away from anomalous flux locations ranged from 10°C to 26°C. Elevated soil temperatures are herein defined as temperatures above 30°C. Elevated soil temperatures were observed during the spring 1998 field campaign in the SG and MF grids with maximum temperatures of 96° and 70°C, respectively. During the fall 1998 campaign, the same locations in the SG and MF grids again exhibited the maximum soil temperatures, but the temperatures had declined to 80°C and 60°C, respectively. Maximum soil temperatures around 97°C were recorded at several fumarole locations along the RF fault zone. Soil temperatures at fumaroles in the RF grid showed no change during this time.

The soil temperature data presented in Fig. 8 are from all three field campaigns and have been separated into three groups consisting of sites from the range front, alluvial fans and the basin. As a whole the data show a great deal of scatter but indicate a modest positive correlation between temperature and flux ($r = 0.68$). This relation is supported mostly by data from the range front and basin sites. There is less correlation between flux and temperature from the MF sites.

4.3. Gas geochemistry

All of the fumaroles sampled, except Figure Eight fumarole, are located in the dead zone (Fig. 2). The

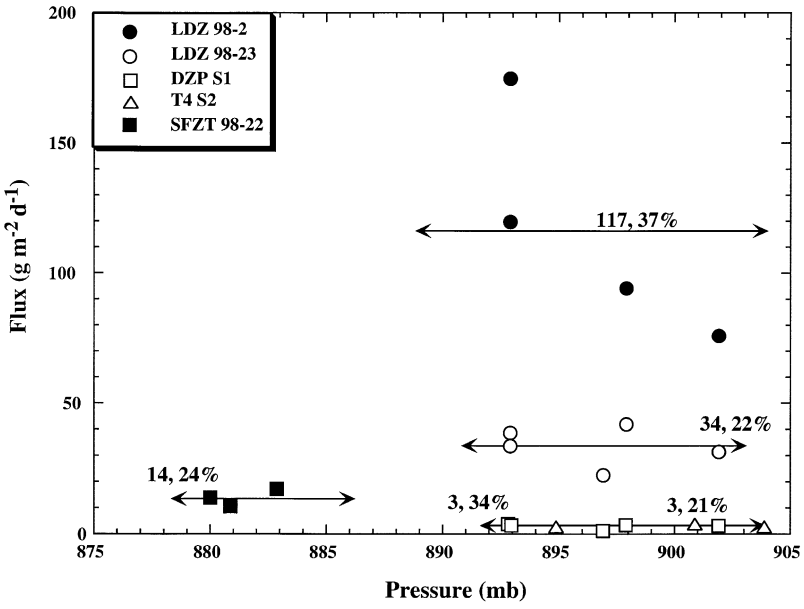

Fig. 7. Plot showing the difference in CO_2 flux measurements from five locations, taken on different days. Only the high flux site shows a relation between flux and atmospheric pressure. Numbers above the lines give the average flux value and the coefficient of variation (%) for the replicate measurements.

gases from the fumaroles are similar to those found in the geothermal production wells (Table 2). Fumarole samples generally contain more than 99 mol% water, and the non-condensable fractions contain

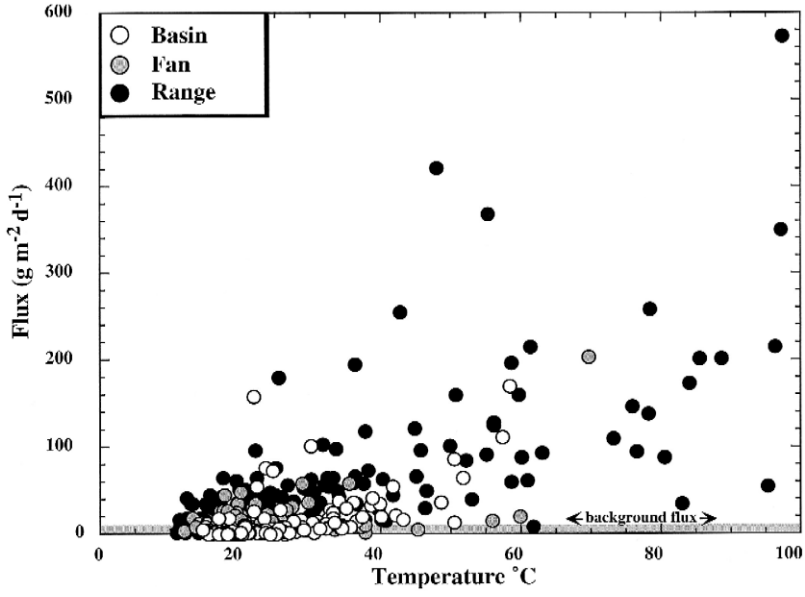

Fig. 8. Plot of soil temperature vs. CO_2 flux for data from all field campaigns. Samples from the SG, MF and RF grids are included in the basin, fan, and range designations, respectively.

Table 2
Composition of gases from fumaroles and geothermal wells at Dixie Valley, NV, and $^{13}C–CO_2$ data on selected samples. Unless otherwise noted, values are in mol% dry gas

	Fumaroles and vents									Wells	
Location	Senator	Senator	Senator	Calcite	Calcite	S. Bench	Lonely	Crack 4	Figure Eight	46-32 Well	Production wells[a]
Sample #	DV9744	DV98-108	DV98-164	DV98-109	DV98-165	DV98-166	DV98-167	DV97-43	DV98-181	DV97-53	–
Date	11/3/97	5/2/98	10/25/98	5/1/98	10/25/98	10/27/98	10/27/98	11/3/97	10/29/98	11/4/97	–
Temperature (°C)	97.3	97.1	96.5	95.8	97.0	97.4	96.4	97.6	97.4	155.0	–
CO_2	91.8	96.5	91.0	96.0	94.0	92.1	97.2	94.4	31.1	97.8	95.4
H_2S	1.27	0.52	0.57	0.74	0.72	1.03	0.42	0.75	0.07	0.36	0.84
H_2	0.18	0.34	0.16	0.67	0.41	0.23	0.55	1.23	0.09	1.45	0.02
CH_4	0.12	0.23	0.19	0.10	0.10	0.21	0.14	0.11	< 0.007	0.08	0.55
NH_3	1.50	0.14	1.02	1.6	1.43	0.02	< 0.0004	0.11	0.01	0.05	0.55
N_2	4.08	1.82	5.42	0.86	2.69	5.21	1.62	3.15	53.6	0.23	1.16
Ar	0.081	0.039	0.112	0.021	0.051	0.104	0.027	0.072	0.647	0.006	0.027
O_2	0.847	0.034	1.460	0.001	0.202	0.853	0.055	0.180	14.659	0.002	0.014
He	0.0011	0.0012	< 0.0008	0.0003	0.0007	0.0013	0.0010	0.0002	< 0.007	< 0.0002	0.0021
Hg	0.004	0.0004	0.0003	na	0.0002	0.00002	0.000004	na	0.000002	0.0003	0.0001
Mol% H_2O	99.8	99.7	99.8	99.6	99.6	99.8	96.7	99.6	76.1	96.5	99.7
$^{13}C–CO_2$	−5.4‰	−5.3‰	na	−3.6‰	na	na	na	−4.4‰	na	−4.5‰	−4.8‰[b]
Gas Geothermometers temperatures (°C)[c]											
$CO_2–H_2S–H_2–CH_4$	201	200	187	229	216	201	213	245	204[d]	241	196
$H_2–Ar$	198	240	186	280	238	198	267	261	115	342	166

Carbon isotope analyses were performed by M. Huebner (USGS) in the laboratory of C.J. Janik. Mass spectrometry was provided by L.D. White (USGS, Menlo Park, CA). Gas analyses by D. Counce (LANL) and C.J. Janik using procedures described in Fahlquist and Janik (1992) and Werner et al. (1997).

[a]Average of 12.

[b]^{13}C data is from a separate set of 18 samples. The analyses are reported in permil relative to the PDB standard; 1σ standard deviation ± 0.2‰.

[c]D'Amore and Panichi (1980) and Giggenbach and Goguel (1989), respectively.

[d]Maximum value.

roughly 94 mol% CO_2, ≤ 1 mol% H_2S, ≤ 1 mol% H_2, and ≤ 0.2 mol% CH_4. Admixed air is present in nearly all fumarole samples, particularly in Figure Eight fumarole, a recently identified, low-pressure vent about 1 km northeast of the dead zone on the Stillwater Fault. This fumarole also contains the least water vapor. Some fumarole samples contain slightly high NH_3, possibly from thermal decomposition of vegetation in the dead zone area. All samples contain very low, but detectable Hg (≤ 0.004 mol%). The shallow 46-32 geothermal test well is also located in the dead zone. This well is usually shut in. When flowing, it only produces steam and contains anomalous H_2, probably from reaction of hot fluid with the iron casing.

Gas geothermometers indicate subsurface temperatures of 115°C to 342°C (Table 2). The excess H_2 in well 46-32 and atmospheric Ar in the Figure Eight

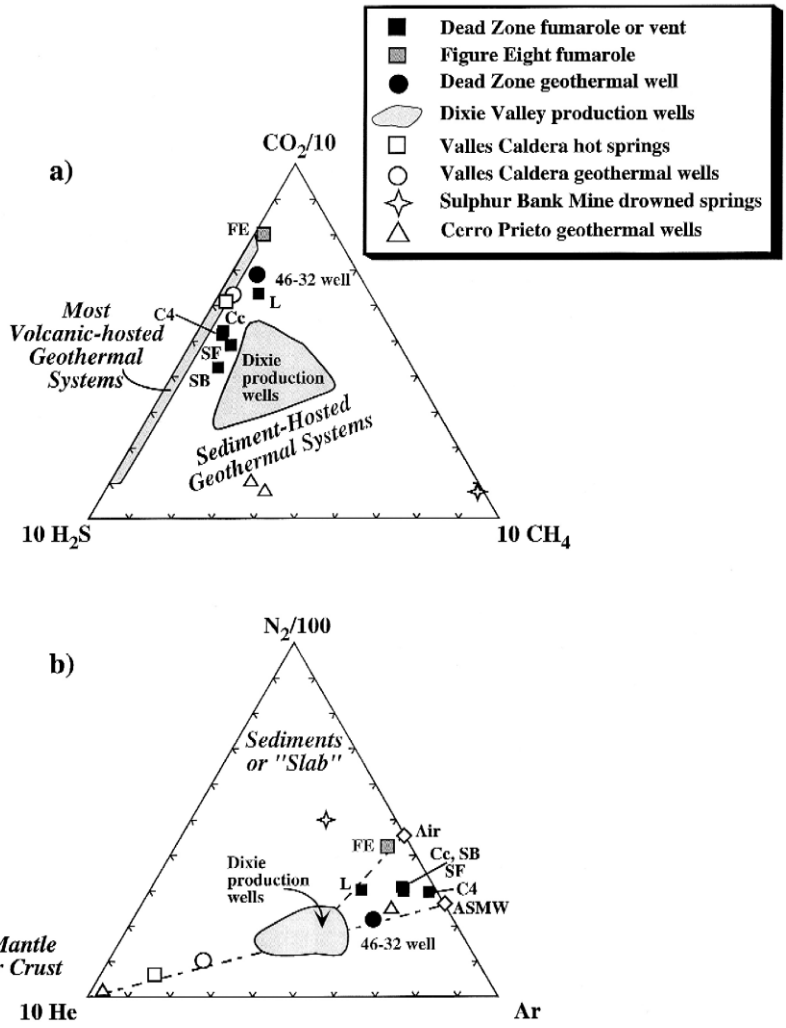

Fig. 9. Ternary plots of DV gases. (a) CO_2–H_2S–CH_4 plot. (b) N_2–He–Ar plot. C4 = Crack 4 located in the SG grid is an average of two analyses; the fumaroles are labeled as in Fig. 2; the SF composition is an average of three analyses. Dashed lines show mixing between He-rich component and ASMW and between DV reservoir gases and air. Valles Caldera (New Mexico) points are averages of 34 intracaldera hot spring and fumarole analyses and 27 geothermal well analyses. Sulphur Bank Mine points are the average of seven hot spring analyses. Cerro Prieto points are averages of 27 and 35 geothermal well samples from 1982 and 1991, respectively. He concentrations for FE and the 46-32 well were plotted using the less than value. If zero He is assumed, the samples plot at air and ASMW. Data from this paper, Nehring and D'Amore (1984), and Goff and Janik (1993, 2000, in preparation).

Table 3
Stable isotope data from dead zone fumaroles and DV geothermal wells, and the vapor fractin for brine/steam pairs

Sample #	Well #	Date	Type location	Vapor fraction	δD brine	δ^{18}O brine	δD steam	δ^{18}O steam
DV97-25,27	27-33	10/30/97	Production well	0.16	−128	−14.0	−135	−16.8
DV98-75,76	27-33	04/28/98	Production well	0.15	−126	−13.9	−134	−16.8
DV98-133,134	27-33	10/20/98	Production well	n/a	−129	−14.0	−135	−16.9
DV98-135,136	27-33 off line	10/20/98	Production well	0.19	−127	−13.8	−137	−17.1
DV97-30,31	28-33	10/30/97	Production well	0.16	−126	−13.7	−134	−16.4
DV98-79/101	28-33	04/28/98	Production well	0.16	−127	−13.8	−133	−16.5
DV98-141,142	28-33	10/21/98	Production well	0.16	−127	−13.7	−134	−16.6
DV99-200,201	28-33	5/5/99	Production well	0.16	−127	−13.7	−133	−16.5
DV97-29,28	37-33	10/30/97	Production well	0.16	−129	−13.8	−134	−16.6
DV98-77,78	37-33	04/28/98	Production well	0.16	−127	−13.8	−131	−16.5
DV98-140,139	37-33	10/21/98	Production well	0.16	−127	−13.8	−134	−16.7
DV99-199,202	37-33	5/5/99	Production well	0.16	−126	−13.8	−134	−16.6
DV98-86,87	63-7	04/28/98	Production well	0.15	−125	−13.1	−132	−16.0
DV98-147,149	63-7	10/22/98	Production well	0.16	−124	−13.0	−132	−15.9
DV99-188,189	63-7	5/4/99	Production well	0.15	−125	−13.0	−131	−15.9
DV97-11,12	73-7	10/29/97	Production well	0.16	−126	−13.2	−130	−15.1
DV98-88,89	73-7	04/29/98	Production well	0.15	−125	−13.1	−125	−13.6
DV98-152,153	73-7	10/22/98	Production well	0.15	−125	−13.0	−129	−15.3
DV99-190,191	73-7	5/4/99	Production well	0.15	−124	−12.9	−130	−15.1
DV97-23,22	73B-7	10/30/97	Production well	0.16	−125	−13.1	−132	−15.5
DV98-95,94	73B-7	04/29/98	Production well	0.15	−126	−13.2	−131	−16.0
DV98-154,155	73B-7	10/22/98	Production well	0.15	−126	−13.1	−133	−15.7
DV99-197,192	73B-7	5/5/99	Production well	0.15	−124	−13.0	−127	−14.5
DV97-14,15	74-7	10/29/97	Production well	0.16	−126	−13.4	−133	−15.8
DV98-84,85	74-7	04/28/98	Production well	0.16	−125	−13.3	−133	−16.2
DV98-150,151	74-7	10/22/98	Production well	0.16	−126	−13.2	−133	−16.1
DV99-184,185	74-7	5/4/99	Production well	0.16	−126	−13.1	−131	−15.7
DV96-8,7a	76-7	10/25/96	Production well	0.16	−122	−14.1	−130	−16.9
DV98-145,144	76-7	10/22/98	Production well	0.16	−126	−13.3	−133	−16.2
DV98-80,81	76A-7	04/28/98	Production well	0.19	−125	−13.3	−132	−16.2
DV99-182,183	76A-7	05/04/99	Production well	0.16	−125	−13.2	−133	−16.1
DV97-20,21	82A-7	10/29/97	Production well	0.16	−127	−13.2	−126	−13.6
DV98-90,91	82A-7	04/29/98	Production well	0.15	−125	−13.2	−128	−14.6
DV98-156,157	82A-7	10/23/98	Production well	0.15	−125	−13.1	−133	−15.8
DV99-196,195	82A-7	5/4/99	Production well	0.15	−125	−13.1	−131	−15.7
DV96-9,10a	V101	10/25/96	Production separator	0.16	−123	−14.3	−129	−17.2
DV97-26,24	V101	10/30/97	Production separator	0.16	−129	−13.7	−135	−16.5
DV98-73,74	V101	04/28/98	Production separator	0.16	−126	−13.8	−133	−16.6
DV-138,137	V101	10/21/98	Production separator	0.17	−127	−13.7	−134	−16.6
DV99-204,203	V101	5/5/99	Production separator	0.16	−128	−13.7	−134	−16.6
DV97-16,17	V102 + 103	10/29/97	Production separator	0.16	−126	−13.2	−133	−16.2
DV98-82,83	V102 + 103	04/28/98	Production separator	0.15	−124	−13.2	−131	−16.0
DV98-148,146	V102 + 103	10/22/98	Production separator	0.16	−125	−13.1	−132	−16.0
DV99-186,187	V102 + 103	5/4/99	Production separator	0.20	−125	−13.1	−132	−16.0
DV97-18,19	V105	10/29/97	Production separator	0.16	−125	−13.2	−133	−16.1
DV98-92,93	V105	04/29/98	Production separator	0.14	−124	−13.1	−133	−16.0
DV98-159,158	V105	10/23/98	Production separator	0.16	−125	−13.1	−132	−15.9
DV99-194,193	V105	5/5/99	Production separator	0.14	−124	−13.0	−131	−15.9
DV97-55,54	27-32	11/5/97	Test well in dead zone	n/a	−126	−14.1	−134	−16.1
DV97-53	46-32	11/04/97	Test well in dead zone	n/a	–	–	−161	−22.3
DV98-100	46-32	04/29/98	Test well in dead zone	n/a	–	–	−148	−19.2
DV97-44	Senator fumarole	11/03/97	Dead zone fumarole	n/a	–	–	−137	−17.5

Table 3 (*continued*)

Sample #	Well #	Date	Type location	Vapor fraction	δD brine	δ^{18}O brine	δD steam	δ^{18}O steam
DV98-108	Senator fumarole	5/1/98	Dead zone fumarole	n/a	–	–	−145	−19.1
DV97-43	Crack 4 vent	11/03/97	Vent in steaming ground	n/a	–	–	−155	−20.1
DV98-124	Crack 4 vent	5/6/98	Vent in steaming ground	n/a	–	–	−160	−21.4
DV98-109	Calcite fumarole	5/1/98	Dead zone fumarole	n/a	–	–	−161	−21.4
DV98-165	Calcite fumarole	10/25/98	Dead zone fumarole	n/a	–	–	−167	−21.9
DV98-166	South Benche fumarole	10/26/98	Dead zone fumarole	n/a	–	–	−166	−22.9

Sample numbers are reported for brine and steam condensate samples, respectively.
Isotope analyses were performed in the laboratory of T. Coplen (USGS, Restson, VA) using the hydrogen and CO_2 equilibration techniques of Coplen et al. (1991) and Epstein and Mayeda (1953) for δD and δ^{18}O, respectively. Values are relative to the SMOW standard; 1σ standard deviation is $\pm$1‰ for δD and $\pm$1‰ for δ^{18}O. n/a: Not available.

fumarole influence the temperature estimates; without these samples, the calculated temperatures range between 166°C and 280°C. Measured temperatures as hot as 155°C occur at only 100 m depth on the south edge of the dead zone in the 46-32 well. The DV geothermal reservoir has a maximum fluid-entry temperature of about 250°C (Benoit and Hirtz, 1994), but the geothermometers indicate maximum gas equilibrium temperatures of about 200°C.

Major gas contents at DV are compared to those from some other geothermal systems in Fig. 9a, a ternary plot of CO_2–H_2S–CH_4. DV gases contain somewhat more CH_4 than most volcanic-hosted geothermal systems such as Valles Caldera (New Mexico), but contain less CH_4 than reservoirs hosted in organic-rich sediments such as Cerro Prieto (Baja California, Mexico) and Sulphur Bank Mine (California). The DV geothermal reservoir consists of faulted Triassic metaquartzites and Jurassic gabbroic rocks, although sedimentary rocks with possible organic components underlie and overlie the reservoir. Hulen et al. (1999) studied hydrocarbon droplets in some DV production wells and concluded that the oil migrated into the reservoir from local Tertiary-aged lacustrine source rocks. Even so, the CH_4 contents of DV gases are quite low compared to typical oil field gases.

Inert gas contents at DV are shown in the ternary N_2–He–Ar plot of Fig. 9b. DV production well gases lie on the mixing line between air-saturated meteoric water (ASMW) and mantle (or crustal) end members. The 46-32 well contains additional N_2 and Ar from ASMW. The Lonely and Figure Eight fumaroles lie on a mixing line between production well gas compositions and air. Crack 4 (C4), Senator, South Bench, and Calcite fumaroles show mixing between well gases and both air and ASMW. Despite the fact that these samples contain some air contamination, their positions in Fig. 9b also show admixture of ASMW.

DV gases contain substantially less He than gases from typical volcanic-hosted geothermal systems, such as Valles Caldera. Previously reported R/R_a values for gases in the DV production wells of ≤ 0.76 (Kennedy et al., 1996), and the gas ratios in Fig. 9b suggest that DV He may originate by mixing of He in ASMW ($R/R_a = 1$) with He from crustal decay of U and Th ($R/R_a \leq 0.2$, (Hoke et al., 1994)). A magmatic/mantle source of He is not indicated.

4.4. Stable isotopes

Oxygen and hydrogen isotope analyses were performed on the following types of water samples: (1) brine and steam-condensate sample pairs from the geothermal wells, (2) meteoric waters from cold springs and shallow cold water wells from locations in and around the geothermal field, and (3) steam-condensate samples from fumaroles in and around the dead zone and C4 in the SG grid. There are no hot or cold springs within the DV geothermal field.

The samples have a wide range in oxygen and hydrogen isotope compositions with the highest values measured on the brine samples from the geothermal wells and the lowest values measured on the steam condensate samples from the fumaroles (Table

3, Fig. 10a). Regional cold meteoric waters form a cluster that is more or less parallel to and enriched by 1.0‰ to 1.5‰ in $\delta^{18}O$ relative to the world meteoric water line of Craig (1961) (Fig. 10a). Lin-

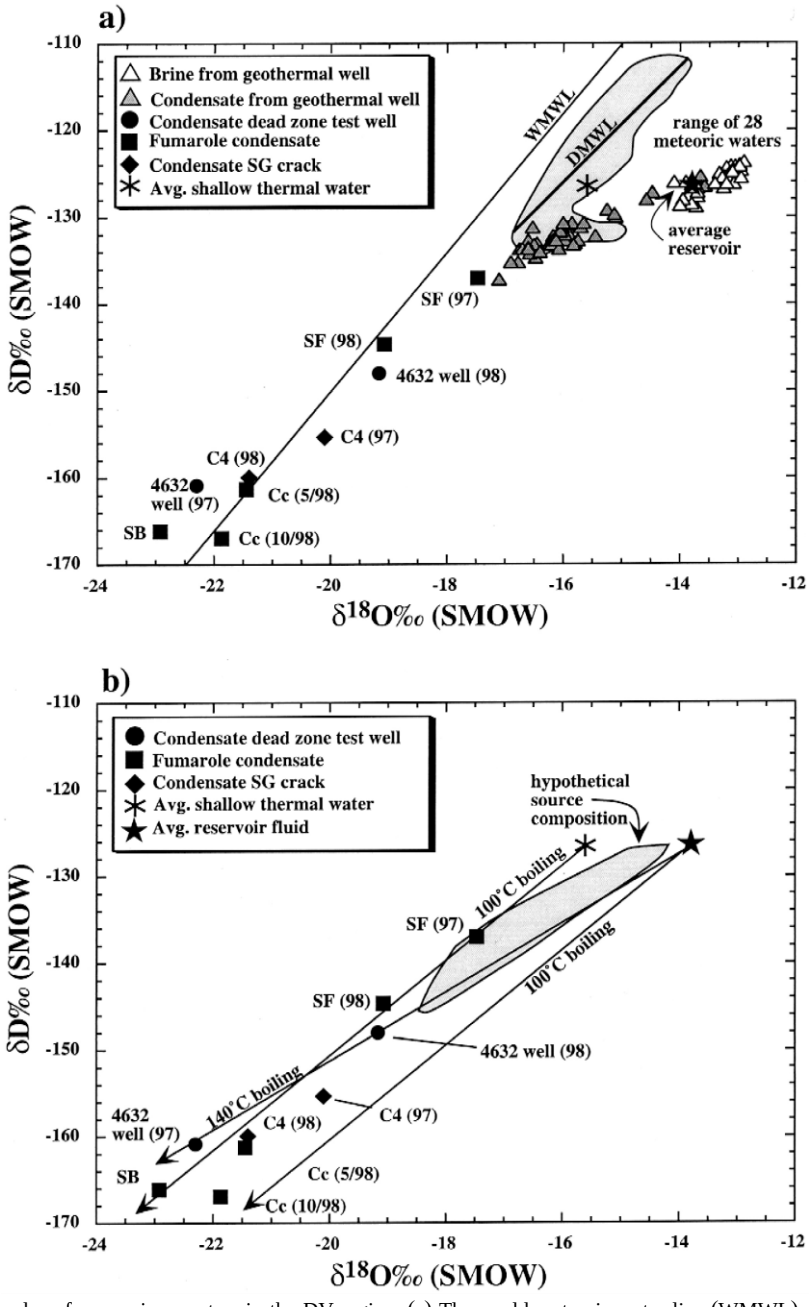

Fig. 10. δD and $\delta^{18}O$ values from various waters in the DV region. (a) The world meteoric water line (WMWL) and DV meteoric water line (DMWL) are shown for reference. Labels are as defined in Figs. 2 and 9, fumarole and vent samples with multiple analyses are identified by year in parentheses. (b) 100°C boiling trends as defined by the isotopic composition of local groundwater and reservoir fluid. Gray cloud represents the range in isotopic compositions for hypothetical parent fluids for SB, Cc, and C4 at 100°C, 46-32 well at 140°C and SF at 160°C.

ear regression of the stable isotope data from 28 cold meteoric waters from locations in the Clan Alpine, Augusta, and Stillwater ranges yields a local meteoric water line equal to $\delta D = 6.68 \times \delta^{18}O - 19.4$ ($r = 0.79$). The low slope of the Dixie meteoric water line is typical of other arid regions where high levels of evaporation occur in enclosed basins (Gat, 1996).

The differences in the stable isotope values of the brine/steam condensate pairs reflects the isotopic fractionation that occurs when the reservoir fluid boils and a steam phase separates from the liquid. The degree of isotopic fractionation is affected by the temperature at which boiling occurs. If boiling occurs at temperatures below 221°C, deuterium and ^{18}O will preferentially partition into the brine phase, while at higher temperatures, deuterium will partition into the steam (Truesdell and Hulston, 1980). Lower separation temperatures result in larger amounts of fractionation between the steam and liquid (Hoefs, 1980).

For fumaroles, isotopic fractionation is also affected by the process of phase separation. If, as a boiling fluid ascends from depth, the steam and brine stay in contact and only separate at a single temperature near the surface, maximum isotopic fractionation will occur between the two phases (Truesdell et al., 1977). In contrast, continuous separation of the two phases will yield minimum isotopic fractionation effects; multiple-stage steam separation effects are intermediate (Truesdell et al., 1977).

Henley et al. (1984) describe the calculations for determination of reservoir conditions from well samples assuming that fluid flow to the surface is rapid and that heat in the reservoir fluid is conserved. If the reservoir temperature is known and the phase separation temperature is determined, then the mass fractions of steam and brine can be calculated from enthalpy balance equations. The stable isotope composition for the reservoir fluid can then be calculated from the isotopic composition of the brine/steam sample pairs using isotope mass balance equations.

For this study, the in-line pressure at the sampling point was used to determine the enthalpy values for the production well samples. Production separator temperatures were provided by power plant operators. The phase separation temperatures for DV production fluids range between 162°C and 168°C. Because some wellbore heat loss does occur as the reservoir fluids are produced, power plant operators also provided wellhead enthalpy data to calculate more accurate steam fractions (Table 3). Assuming single stage boiling, the stable isotope data from 46 brine/steam pairs (collected from 13 wells over 4 years) yield average $\delta^{18}O$ and δD values for the geothermal reservoir fluid of -13.8 ± 0.4‰, and -127 ± 1.4‰, respectively (shown by star in Fig. 10a).

The stable isotope composition of steam condensate samples from five dead zone locations including three fumaroles, C4, and the 46-32 well are also shown in Fig. 10a. Steam from the 1997 sample of SF, the largest and most vigorous fumarole in the area, falls at the end of the trend defined by steam from the geothermal wells. The similarity in the stable isotope composition of this SF steam and the deep well steam is striking, and indicates that the steam at SF is probably derived from high-temperature boiling of a reservoir type fluid. If we assume a reservoir source and isotopic equilibrium between the water and steam fractions, the values for $\delta D_{reservoir} - \delta D_{steam}$ and $\delta^{18}O_{reservoir} - \delta^{18}O_{steam}$ provide information regarding separation temperatures. Assuming single stage separation and using the fractionation factors of Horita and Wesolowski (1994), the apparent separation temperatures for SF steam are 160°C and 144°C from hydrogen and oxygen isotope compositions, respectively. These temperatures are slightly less than the temperatures determined for the well samples from pressure/enthalpy relations.

The stable isotope compositions of steam from the remaining low-pressure fumaroles, the 46-32 well, and a more recent sample of SF have much lower δD and $\delta^{18}O$ values than steam from SF in 1997. These lower values may indicate any one or a combination of the following processes: boiling from a mixed source fluid, multiple boiling events, or lower boiling temperatures. As previously discussed the gas chemistry indicates the fumarolic emissions have a component of air or ASMW (Fig. 9b). The presence of young meteoric fluids in the dead zone is also supported by a tritium value of 0.41 T.U. from water in the shallow 27-32 test well located on the margin of the dead zone. By comparison, seven production wells contain an average of 0.27 T.U.

All of the fumarole samples fit reasonably well within 100°C boiling trajectories projected from groundwater and reservoir source fluids (Fig. 10b). Steam from the 46-32 well falls along a 140°C boiling trend from the reservoir fluid. Downhole temperatures measured in the well range between 142°C and 155°C. Calculation of the initial isotope composition of fluids in equilibrium with the steam from the fumaroles and the well yields hypothetical parent waters with a large range in δD and δ^{18}O values. Fumaroles at some other geothermal systems also show large ranges in isotope compositions. These variations have been attributed to subsurface condensation of steam and multiple occurrences of low temperature boiling (Goff et al., 1991, 1992). Similar processes may be affecting the isotope composition of dead zone steam at DV. Although the stable isotope compositions of the steam do not pinpoint the source fluid they are consistent with boiling of reservoir fluid and varying proportions of ASMW.

Carbon isotope analyses were performed on CO_2 gas from production wells, the 46-32 well, two dead zone fumaroles, and the C4 vent. $\delta^{13}C$–CO_2 values for two samples from SF and one from Calcite fumarole are −5.4‰, −5.3‰ and −3.6‰, respectively (Table 2). These values span the average carbon isotope composition of CO_2 in the production wells (−4.8‰). The $\delta^{13}C$–CO_2 values for C4 and the 46-32 well are nearly identical to CO_2 from the production wells suggesting a similar source for the CO_2 in deep fluids and the fumaroles.

The carbon isotope values of DV CO_2 indicate that it is derived from a relatively ^{13}C-rich source and is not likely related to thermal degradation of organic material like CO_2 in The Geysers geothermal system (Bergfeld et al., 2001). The $\delta^{13}C$–CO_2 values are within the range for mantle-derived CO_2 (Hoefs, 1980), but as discussed earlier, there is no compelling evidence for mantle-derived fluids at DV. The geothermal reservoir CO_2 is also inconsistent with formation by thermal decarbonation of regional Triassic limestone possibly underlying crystalline reservoir rocks ($\delta^{13}C = +1.3$‰, average of two samples). CO_2-calcite isotope equilibria between the limestone and DV CO_2 yield temperature estimates that are < 100°C.

Calcite veins from multiple hydrothermal events are abundant in rocks exposed in the Stillwater Range and in the fault gouge and breccia zones adjacent to the fumaroles. We analyzed four calcite veins from a gabbro, quartzite, argillite and fault gouge. $\delta^{13}C$ values for the veins fall between −4.3‰ and −3.9‰. Temperatures calculated from CO_2-calcite isotope equilibria using the average $\delta^{13}C$-calcite value of −4.0‰ and the $\delta^{13}C$ values of the DV CO_2 are between 150°C and 200°C. The temperature estimates are reasonable for the DV geothermal system and provide convincing evidence that the CO_2 is produced by thermal decarbonation of early hydrothermal calcite in the reservoir rocks.

5. Discussion

5.1. Behavior of the dead zone

During the fall 1998 field campaign it became apparent that changes were occurring in the MF and SG grids. It became rare to observe any steam rising from the dead zone cracks, and the soil temperatures at hot spots in the SG and MF grids had declined. In addition, sample localities where the flux formerly had quickly over-ranged the measurement capabilities of the IRGA were no longer problematic to sample.

An increase in soil moisture could create conditions that would result in a decrease in the measured CO_2 flux. These conditions are temporary and are reflective of a decrease in the soil pore space and are influenced by the pore waters ability to absorb CO_2 (Hinkle, 1994). The fall 1998 field campaign was generally dry with 1 day out of 11 lost to rain. The conditions during the spring were wetter with three nighttime rainstorms in 8 days of field work. Since conditions were generally wetter in the spring, but the spring flux was higher, we do not feel that soil moisture was a factor in the lower fluxes observed during the fall 1998 study.

The fact that the drop in flux in the SG and MF grids was localized instead of resulting from an overall decline at all sites, suggests that the excess CO_2 had been focused along discrete pathways. As such, the decline in flux could indicate that the pathways for the gas had become blocked. This blockage could result from mineral precipitation, the formation of clays or increased soil compaction due

to subsidence. In contrast to the lower elevation sites, the flux in the RF grid showed a smaller decline. If the CO_2 pathways had become blocked, the difference between the three areas could be explained by greater permeability along the Stillwater Fault.

The time span between the formation of the dead zone to the end of this study was about 3 years. Although surface precipitates/sublimates were observed in association with ground cracks, it is unlikely that enough alteration could have occurred to be responsible for the large drop in the CO_2 flux. Ground subsidence, however, has been documented in the DV basin and increased compaction may have cut off former gas pathways. In either case, if a physical process was the cause of the flux decline, the CO_2 would likely migrate along alternative paths to the surface. If the new discharge areas were outside of the 1998 field campaign, they would not be detected by this study. It should be noted, however, that there have been no new areas of SG or dying vegetation observed since the study began.

The drop in flux possibly reflects a change in the processes that first created the excess CO_2 and the initial development of the dead zone. As a geothermal field is produced, reservoir conditions change. Between September 1988 and January 1999, over 1.5×10^8 metric tonnes of flashed brine have been injected into the geothermal reservoir at DV, altering the chemical composition of the fluids in different sections of the field (Kennedy et al., 1999). In spite of the injection, the fluid pressure in the reservoir has declined. It is generally believed that both sets of ground cracks near the margins of the DV geothermal field have resulted from basin subsidence related to fluid withdrawal and lower pressure in the reservoir (Bergfeld et al., 1998; Allis et al., 1999; S. Johnson, 1997, personal communication). Subsidence-related extension in the area around the southern cracks may have enhanced subsurface conditions for gas flow. Earlier studies at DV (Bergfeld et al., 1998; Allis et al., 1999) argued that the decrease in the reservoir pressure caused the development of the dead zone. If this is so, the substantial differences in CO_2 flux and soil temperatures at the two sets of ground cracks indicate that the surface effects of the reservoir pressure drawdown were not uniform across the geothermal field.

The gas geochemistry (Fig. 9) shows that fluids emitted from the dead zone contain both geothermal and meteoric components. The hydrogen and oxygen isotope data from the fumaroles, although less definitive than the gas geochemistry, is best explained by low temperature boiling of a combined geothermal/groundwater source. $\delta^{13}C$ values for CO_2 in dead zone steam indicate a similar CO_2 source for the fumarole fluids and the production wells. The similarity in the chemistry of the fluids venting at the young SG cracks and those venting from the older fumaroles is a clue that geothermal fluids were likely present beneath all parts of the dead zone. If so, then the formation of the dead zone vents and the reported increased vigor at SF were likely surficial expressions of changes occurring in the underlying reservoir.

5.2. Geothermal reservoir model

Hydrothermal outflow plumes are common features at all types of geothermal systems (Goff et al., 1988; Goff and Janik, 2000). The basic requirements for creation of a hydrothermal outflow plume are convective upflow above a deep source reservoir and lateral flow into a permeable conduit or layer adjacent to, or above the region of upflow. The "classic" Basin and Range outflow occurs at Roosevelt Hot Springs, UT, in which reservoir fluid rises along the Opal Mound Fault cutting crystalline rocks and flows into Quaternary alluvial fan deposits (Goff et al., 1988). There are many geohydrologic parallels between the Roosevelt system and DV.

Based on downhole pressure and temperature data, Allis et al. (1999) modeled development of the dead zone at DV as resulting from upflow of reservoir fluids along the Stillwater Fault, with lateral outflow southeast into alluvial fan deposits. They concluded that the dead zone developed because of the decrease in fluid pressure in the reservoir that caused boiling at greater depths, producing steam in the outflow zone instead of a single-phase fluid. The additional steam produced above the outflow then migrated to the surface, and the increased thermal activity caused the plants to die back.

An intriguing feature at DV was defined early in the study by a northwest–southeast aligned zone of elevated CO_2 flux values that extended from the RF

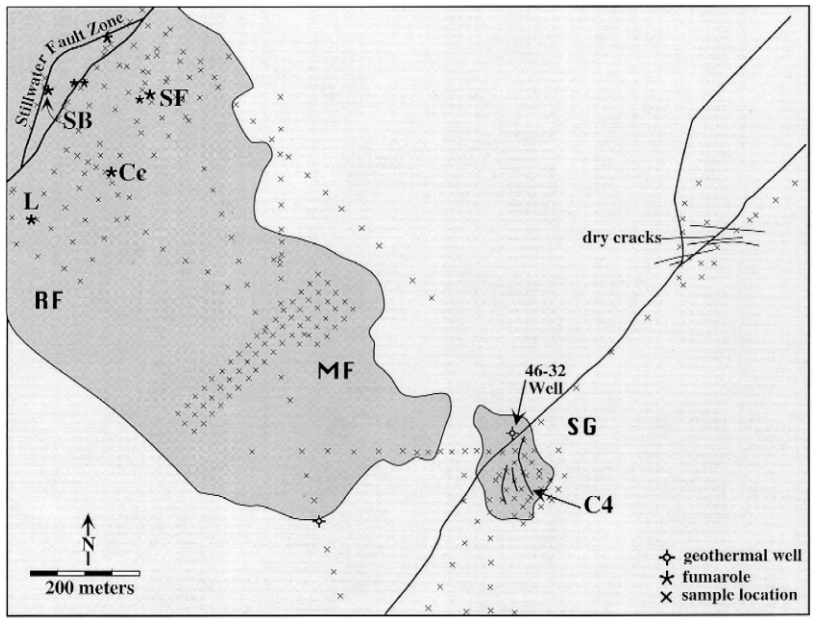

Fig. 11. Composite contour map of CO_2 flux at DV using spring 1998 flux measurements for grid areas and fall 1997 flux measurements for other locations in the basin and across the fans. Gray color highlights the area with CO_2 flux values greater than background (7 g m^{-2} day^{-1}).

out to the SG area (Fig. 11) (Bergfeld et al., 1998). This zone seemingly connects the older established fumaroles with the young features in the MF and the SG. The pattern produced by the elevated CO_2 flux contour is strikingly similar to the contour map of elevated sub-surface temperatures reported by Allis et al. (1999, Fig. 5). The outflow plume concept can also explain the early anomalous CO_2 flux and elevated surface soil temperatures in the dead zone, but must be extended to explain why the flux has subsequently declined.

Our model is shown in two schematic cross-sections in Fig. 12 and builds on the earlier work of Allis et al. (1999) and Goff and Janik (2000) by adding the results from our CO_2 flux and geochemical studies. In the extensional environment of DV, convecting geothermal fluids rise preferentially along the Stillwater fault zone. As they near the surface, some of these fluids $\pm$ shallow groundwater boil at temperatures ≤ 160°C and form steam that is discharged from fumaroles. The elevated CO_2 flux is concentrated in this region. The brine component of this boiling fluid flows laterally from the fault zone into alluvial fan deposits, down gradient towards the basin. By late 1996, drawdown in the reservoir reduced the volume of fluid in the outflow plume, and the lower pressures induced more boiling in the upflow zone. This increased the vigor of existing RF fumaroles and created new ones, including those forming down the fan at the top of the dying outflow plume (Fig. 12a). The increased boiling and associated heat from steam caused vegetation kills in both areas. It also produced large CO_2 fluxes in the RF and created discrete zones of high CO_2 flux down gradient. The reservoir drawdown also caused basin subsidence and formation of two sets of ground cracks near the margin of this subsidence. Because the SG cracks coincide with the zone of induced boiling above the outflow, these cracks provided new but temporary conduits for steam and heat to escape to the surface. By 1998, the upflow zone was so restricted by reservoir drawdown that little fluid entered the outflow plume and excess shallow steam production began to wane (Fig. 12b). On lower sections of the dead zone, the smaller fumaroles became less active and cracks no longer vented steam. Cessation in steam production allowed the vegetation to regenerate.

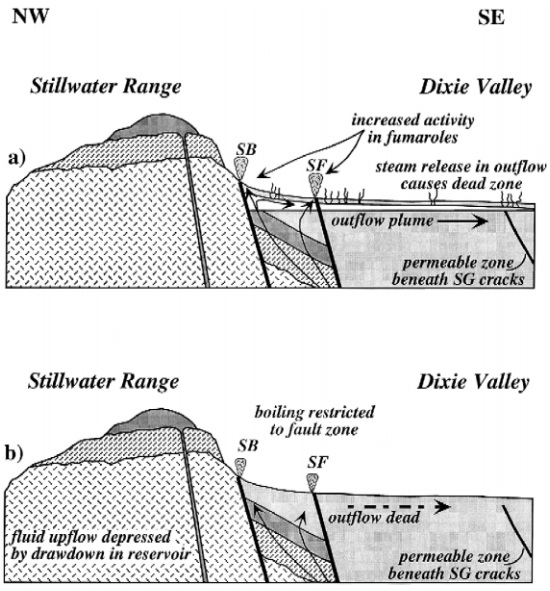

Fig. 12. Schematic NW–SE cross-section showing hydrothermal conditions along the Stillwater Fault and dead zone. (a) 1996: Fluids upflow along faults along the Stillwater Range and have formed an outflow in alluvial fan deposits and underlying lithologies. Drawdown in reservoir causes increased vigor at large fumaroles and induces boiling at the top of the outflow. Production of 1.5×10^{8} t of fluid in reservoir since 1986 caused subsidence in the basin and the formation of ground cracks. Steam produced by boiling of outflow rises along this structure. (b) 1998: Steam production above dead zone wanes as outflow is boiled dry, for lack of fluid upflow.

A possible variation to this model would be that ground-cracking due to subsidence changed the local permeability in the alluvium hosting the outflow plume, and resulting decreases in subsurface pressure allowed the fluid to boil. This boiling was not a steady-state condition; a moving boiling front mined heat from the surrounding rock as it propagated down gradient. Through time, this two-phase zone grew, using up the stored water and energy in the rock. Once the water and heat were consumed, the generation of shallow steam ceased. This model implies that the first occurrence of shallow steam production would move away from the streaming cracks area with time, but the propagation of such a steam front was not observed.

The approximate mass of reservoir fluid required to create the recent CO_2 flux anomaly along the Stillwater fault zone (RF area) can be calculated using the data from Table 2 and reasonable assumptions about the configuration and behavior of the outflow plume. The steam/CO_2 molar ratio for the production wells and the major fumaroles averages about 400 and the steam fraction for 160°C boiling is about 0.16. To produce the CO_2 flux of 7.5 t day^{-1} in April 1998 requires that 15 kg/s of steam was rising along the Stillwater fault zone. This steam could only come from boiling of nearly 80 kg/s of geothermal brine. This value is 16 times greater than the pre-production mass discharge rate of 5 kg/s of brine into the outflow plume calculated by Allis et al. (1999) (their value has a factor of two uncertainty). These results support the model that increased boiling is occurring in the upflow of the reservoir, and that pressure declines have likely reached the point where brine no longer flows up the RF pathways and enters the outflow zone.

The early CO_2 flux in the RF under pre-production conditions can also be estimated if we assume the mass discharge of 5 kg/s from Allis et al. (1999) is approximately correct. Gas data reported by Benoit and Hirtz (1994) show that the original steam/CO_2 ratio of the reservoir fluid was about 170 (98% CO_2 in non-condensable phase and 99.4% steam in total gas). As mentioned above, the reservoir fluid chemistry has changed with production and injection such that the reservoir CO_2 has been depleted by a factor of about two. The pre-production CO_2 flux at RF in 1986, reflecting natural discharge from the geothermal system, was about 1 t day^{-1}. This is about 85% less than the maximum flux of 7.5 t day^{-1} measured in 1998.

6. Conclusions

Three areas of CO_2 degassing were measured in the northern portion of the DV geothermal field between late 1997 and 1998. Degassing of around 7.5 t day^{-1} CO_2 occurred along locations near the Stillwater Fault in the RF grid. An additional 0.5 t day^{-1} of geothermal CO_2 was also emitted from the MF and SG areas. Over the period of the investigation, the CO_2 flux from these lower sections of the study area declined to around half of what was measured earlier. The locations with the most no-

table decreases in flux were from sites near the SG cracks and in a hot zone in the MF grid. Concurrent with the drop in flux, soil temperatures in these areas also declined. The flux in the RF grid may have also decreased but to a much smaller degree. No changes in soil temperatures were observed in the RF area.

Gases from the fumaroles resemble the production well gases in chemical and isotopic composition, but indicate some mixing with air or ASMW. Stable isotope data on most of the fumarole condensates are varied but suggest that steam forms by 100°C boiling of a combined reservoir/shallow groundwater source. Steam from a shallow well in the dead zone and from SF likely forms at higher temperatures between 140°C and 160°C. Carbon isotope data indicate that CO_2 in the wells and fumaroles is derived from thermal degradation of hydrothermal calcite veins.

The geochemical data presented here are consistent with general models of hydrothermal outflow plumes (Goff et al., 1988) and with the model of the DV geothermal system presented by Allis et al. (1999). Declines in reservoir pressure were responsible for increased boiling of ascending fluids along the Stillwater Fault and for suddenly inducing boiling above the outflow plume in 1997 to 1998. We estimate that maximum CO_2 flux along the RF in 1998 was about 7.5 times greater than pre-production CO_2 flux along the same zone in 1986. The increased steam and heat caused die off of vegetation above the outflow path. By 1999, drying out of the outflow caused CO_2 flux and temperature in the dead zone to decrease and allowed vegetation to return.

Acknowledgements

We thank Oxbow Power Services, especially Stuart Johnson and Dick Benoit, who provided access, knowledge, and inspiration during the course of this investigation. In addition, we thank Cheryl Schmitt and the UNM Statistics Clinic for help with statistical models. W.C. Evans and M. Nathenson of the U.S. Geological Survey, Menlo Park, CA, and K. Wohletz of Los Alamos National Laboratory provided helpful reviews and comments that greatly improved the manuscript. This project was supported by the U.S. Department of Energy, Office of Geothermal Technologies (Marshall Reed, project manager) and by grants to D. Bergfeld from the Associated Western Universities and the Office of Graduate Studies at the University of New Mexico, Albuquerque.

References

Allard, P., Carbonnelle, J., Dajlevic, D., Le Bronec, J., Morel, P., Robe, M.C., Maurenas, J.M., Faivre-Pierret, R., Martin, D., Sabroux, J.C., Zettwoog, P., 1991. Eruptive and diffuse emissions of CO_2 from Mount Etna. Nature 351 (6325), 387–391.

Allis, R.G., Johnson, S.D., Nash, G.D., Benoit, D., 1999. A model for the shallow thermal regime at Dixie Valley geothermal field. Geotherm. Resour. Counc., Trans. 23, 493–498.

Anderson, R.E., Zoback, M.L., Thompson, G.A., 1983. Implications of selected subsurface data on the structural form and evolution of some basins in the northern Basin and Range Province, Nevada and Utah. Geol. Soc. Am. Bull. 94 (9), 1055–1072.

Barberi, F., Carapezza, M.L., 1994. Helium and CO_2 soil gas emission from Santorini (Greece). Bull. Volcanol. 56, 335–342.

Benoit, D., Hirtz, P., 1994. Noncondensible gas trends and emissions at Dixie Valley, Nevada. Geotherm. Resour. Counc., Trans. 18, 113–119.

Bergfeld, D., Goff, F., Janik, C.J., Johnson, S.D., 1998. CO_2 flux measurements across portions of the Dixie Valley geothermal system, Nevada. Geotherm. Resour. Counc., Trans. 22, 107–111.

Bergfeld, D., Goff, F., Janik, C.J., 2001. Carbon isotope systematics and CO_2 sources in the Geysers-Clear Lake Region, Northern California. Geothermics 30, in press.

Chiodini, G., Frondini, F., Raco, B., 1996. Diffuse emission of CO_2 from the Fossa Crater, Vulcano Island (Italy). Bull. Volcanol. 58 (1), 41–50.

Chiodini, G., Cioni, R., Guidi, M., Raco, B., Marini, L., 1998. Soil CO_2 flux measurements in volcanic and geothermal areas. Appl. Geochem. 13 (5), 543–552.

Christensen, R., 1991. Linear Models for Multivariate, Time Series, and Spatial Data. Springer-Verlag, New York, 310 pp.

Craig, H., 1961. Isotopic variations in meteoric waters. Science 133 (3465), 1702–1703.

Coplen, T.B., Wildman, J.D., Chen, J., 1991. Improvements in the gaseous hydrogen–water equilibration techniques for hydrogen isotope ratio analyses. Anal. Chem. 63, 910–912.

D'Agostino, R.B., 1971. An omnibus test of normality for moderate and large size samples. Biometrika 58, 341–348.

D'Amore, F., Panichi, C., 1980. Evaluation of deep temperatures of hydrothermal systems by a new gas geothermometer. Geochim. Cosmochim. Acta 44 (3), 549–556.

Epstein, S., Mayeda, T., 1953. Variation of O-18 content of water from natural sources. Geochim. Cosmochim. Acta 4, 213–224.

Fahlquist, L.S., Janik, C.J., 1992. Procedures for collecting and

analyzing gas samples from geothermal systems. U.S. Geol. Surv. Open-File Report 92-211, 19 pp.

Farrar, C.D., Sorey, M.L., Evans, W.C., Howle, J.F., Kerr, B.D., Kennedy, B.M., King, C.Y., Southon, J.R., 1995. Forest-killing diffuse CO_2 emission at Mammoth Mountain as a sign of magmatic unrest. Nature 376 (6542), 675–678.

Farrar, C.D., Neil, J.M., Howle, J.F., 1999. Magmatic Carbon Dioxide Emissions at Mammoth Mountain California. U.S. Geol. Surv. Water Resour. Invest. Rpt. 98-4217, 34 pp.

Forster, C.B., Caine, J.S., Schulz, S., Nielson, D.L., 1997. Fault zone architecture and fluid flow: an example from Dixie Valley, Nevada. Proc. 22nd Workshop on Geotherm. Reservoir Engineering, Stanford University Report SGP-TR-155, Stanford, California. pp. 123–130.

Gat, J.R., 1996. Oxygen and hydrogen isotopes in the hydrologic cycle. Earth Planet. Sci. Lett. 24, 225–262.

Gerlach, T.M., Doukas, M.P., McGee, K.A., Kessler, R., 1998. Three-year decline of magmatic CO_2 emissions from soils of a Mammoth Mountain tree kill: Horseshoe Lake, CA, 1995–1997. Geophys. Res. Lett. 25, 1947–1950.

Gerlach, T.M., Doukas, M.P., McGee, K.A., Kessler, R., 2001. Soil efflux and total emission rates of magmatic CO_2 at the Horseshoe Lake tree kill, Mammoth Mountain, California, 1995–1999. Chem. Geol. 177, 101–116.

Giammanco, S., Gurrieri, S., Valenza, M., 1997. Soil CO_2 degassing along tectonic structures of Mount Etna (Sicily); the Pernicana Fault. Appl. Geochem. 12 (4), 429–436.

Giggenbach, W.F., Goguel, R.L., 1989. Collection and analysis of geothermal and volcanic water and gas discharges. New Zealand Chemistry Division, DSIR, Report No. CD2401, 81 pp.

Gilbert, R.O., 1987. Statistical Methods for Environmental Pollution Monitoring. Van Nostrand-Reinhold, New York, 320 pp.

Goff, F., Janik, C.J., 1993. Gas geochemistry and guide for geothermal features in the Clear Lake region, California. In: Rytuba, J.J. (Ed.), Active Geothermal Systems and Gold–mercury Deposits in the Sonoma-Clear Lake Volcanic Fields, California. Soc. Econ. Geologists Guidebk Series 16, pp. 207–261.

Goff, F., Janik, C.J., 2000. Geothermal systems. In: Sigurdsson, H. (Ed.), Encyclopedia of Volcanoes. Academic Press, pp. 817–834.

Goff, F., Janik, C.J., in preparation. Gas chemistry of Valles Caldera region, New Mexico and comparisons with other geothermal gases. J. Volcanol. Geotherm. Res.

Goff, F., Shevenell, L., Gardner, J.N., Vuataz, F.D., Grigsby, C.O., 1988. The hydrothermal outflow plume of Valles Caldera, New Mexico, and a comparison with other outflow plumes. J. Geophys. Res. 93 (6), 6041–6058.

Goff, F., Janik, C.J., Fahlquist, L.S., Adams, A., Roldan, A., Revolorio, M., Trujillo, P.E., Counce, D., 1991. A reevaluation of the Moyuta geothermal system, southern Guatemala. Geotherm. Resour. Counc., Bull. 20 (10), 290–298.

Goff, S.J., Goff, F., Janik, C.J., 1992. Tecuamburro Volcano, Guatemala; exploration geothermal gradient drilling and results. Geothermics 21 (4), 483–502.

Henley, R.W., Truesdell, A.H., Barton Jr., P.B., Whitney, J.A., 1984. Fluid–mineral equilibria in hydrothermal systems. Rev. Econ. Geol. 1, 267 pp.

Hinkle, M.E., 1994. Environmental conditions affecting concentrations of He, CO_2, O_2 and N_2 in soil gases. Appl. Geochem. 9 (1), 53–63.

Hoefs, J., 1980. Stable Isotope Geochemistry. Springer-Verlag, New York, 208 pp.

Hoke, L., Hilton, D.R., Lamb, S.H., Hammerschmidt, K., Friedrichsen, H., 1994. ^{3}He evidence for a wide zone of active mantle melting beneath the Central Andes. Earth Planet. Sci. Lett. 128 (3–4), 341–355.

Horita, J., Wesolowski, D.J., 1994. Liquid-vapor fractionation of oxygen and hydrogen isotopes of water from the freezing to the critical temperature. Geochim. Cosmochim. Acta 58 (16), 3425–3437.

Hulen, J.B., Collister, J.W., Johnson, S.D., Allis, R., 1999. Oils in the Dixie Valley and Kyle Hot Springs Geothermal Systems, Nevada — Potentially Sensitive Indicators of Natural and Induced Reservoir Processes. Proc. Twenty-fourth Workshop on Geotherm. Reservoir Engineering. Stanford University, Stanford California. pp. 1–15.

Kennedy, B.M., Benoit, D., Truesdell, A.H., 1996. A Preliminary Survey of Noble Gases at Dixie Valley, Nevada. Geotherm. Resour. Counc., Trans. 20, 815–819.

Kennedy, B.M., Janik, C.J., Benoit, D., Shuster, D.L., 1999. Natural Geochemical Tracers for Injectate Fluids at Dixie Valley. Proc. 24th Workshop on Geotherm. Reservoir Engineering, Stanford University Report SGP-TR-162, Stanford California. pp. 108–115.

Lutz, S.J., Moore, J.N., Benoit, D., 1997. Geologic framework of Jurassic reservoir rocks in Dixie Valley Geothermal Field, Nevada: Implication from hydrothermal alteration and stratigraphy. Proc. 22nd Workshop on Geothermal Reservoir Engineering, Stanford University Report SGP-TR-155, Stanford, California. pp. 131–139.

McGee, K.A., Gerlach, T.M., 1998. Annual cycle of magmatic CO_2 in a tree-kill soil at Mammoth Mountain, California; implications for soil acidification. Geology 26 (5), 463–466.

Nehring, N.L., D'Amore, F., 1984. Gas chemistry and thermometry of the Cerro Prieto, Mexico. Geothermics 13 (1–2), 75–89.

Nimz, G., Janik, C.J., Goff, F., Dunlap, C., Huebner, M., Counce, D., Johnson, S.D., 1999. Regional hydrology of the Dixie Valley geothermal field, Nevada: preliminary interpretations of chemical and isotopic data. Geotherm. Resour. Counc., Trans. 23, 333–338.

Norman, J.M., Garcia, R., Verma, S.B., 1992. Soil surface CO_2 fluxes and the carbon budget of a grassland. J. Geophys. Res. 97 (D17), 18845–18853.

Okaya, D.A., Thompson, G.A., 1985. Geometry of Cenozoic extensional faulting; Dixie Valley, Nevada. Tectonics 4 (1), 107–125.

Rogie, J.D., Kerrick, D.M., Chiodini, G., Sorey, M., Virgili, G., 1998. Continuous monitoring of diffuse CO_2 degassing, Horseshoe Lake, Mammoth Mountain, California. EOS Trans. Am. Geophys. Union 79 (45), 942, (abstract).

Shapiro, S.S., Wilk, M.B., 1965. An analysis of variance test for normality (complete samples). Biometrika 52, 591–611.

Sinclair, A.J., 1974. Selection of threshold values in geochemical data using probability graphs. J. Geochem. Explor. 3 (2), 129–149.

Speed, R.C., 1976. Geologic map of the Humboldt Lopolith and surrounding terrane, Nevada. Geol. Soc. Am. Map Chart Ser. MC-14, (1 sheet).

Truesdell, A.H., Hulston, J.R., 1980. Isotopic evidence on environments of geothermal systems. In: Fritz, P., Fontes, J.C. (Eds.), Handbook of Environmental Isotope Geochemistry. Elsevier, pp. 179–226.

Truesdell, A.H., Nathenson, M., Rye, R.O., 1977. The effects of subsurface boiling and dilution on the isotopic compositions of Yellowstone thermal waters. J. Geophys. Res. 82 (26), 3694–3704.

Waibel, A.F., 1987. An overview of the geology and secondary mineralogy of the high temperature geothermal system in Dixie Valley, Nevada. Geotherm. Resour. Counc., Trans. 11, 479–486.

Werner, C., Janik, C.J., Goff, F., Counce, D., Johnson, L., Siebe, C., Delgado, H., Williams, S.N., Fischer, T.P., 1997. Geochemistry of summit fumarole vapors and flanking thermal/mineral waters at Popocatepétl Volcano, Mexico. Los Alamos National Laboratory Report LA-13289-MS, 33 pp.

Werner, C., Brantley, S.L., Boomer, K., 2000. CO_2 emission related to the Yellowstone volcanic system, USA: II. Statistical sampling, total degassing, and transport mechanisms. J. Geophys. Res. 105 (B5), 10831–10846.